Polymer 50 (2009) 4101–4111

Contents lists available at ScienceDirect

Polymer

journal homepage: www.elsevier.com/locate/polymer

Structural evolution of tensile deformed high-density polyethylene at elevated temperatures: Scanning synchrotron small- and wide-angle X-ray scattering studies

Zhiyong Jiang [a], Yujing Tang [a], Jens Rieger [b], Hans-Friedrich Enderle [c], Dieter Lilge [c], Stephan V. Roth [d], Rainer Gehrke [d], Zhonghua Wu [e], Zhihong Li [e], Yongfeng Men [a,*]

[a] State Key Laboratory of Polymer Physics and Chemistry, Changchun Institute of Applied Chemistry, Chinese Academy of Sciences, Graduate School of Chinese Academy of Sciences, Renmin Street 5625, 130022 Changchun, PR China
[b] BASF SE, Polymer Physics, 67056 Ludwigshafen, Germany
[c] Basell Polyolefine GmbH, R&D, 65926 Frankfurt, Germany
[d] HASYLAB am DESY, Notkestr. 85, 22607 Hamburg, Germany
[e] Beijing Synchrotron Radiation Facility, Institute of High Energy Physics, Chinese Academy of Sciences, Beijing 100039, PR China

ARTICLE INFO

Article history:
Received 25 February 2009
Received in revised form
24 April 2009
Accepted 15 June 2009
Available online 1 July 2009

Keywords:
SAXS
Polyethylene
Deformation

ABSTRACT

The structural evolution of an ice-quenched high-density polyethylene (HDPE) subjected to uniaxial tensile deformation at elevated temperatures was examined as a function of the imposed strains by means of combined synchrotron small-angle X-ray scattering (SAXS) and wide-angle X-ray scattering (WAXS) techniques. The data show that when stretching an isotropic sample with the spherulitic structure, intralamellar slipping of crystalline blocks was activated at small deformations, followed by a stress-induced fragmentation and recrystallization process yielding lamellar crystallites with their normal parallel to the stretching direction. Stretching of an isothermally crystallized HDPE sample at 120 °C exhibited changes of the SAXS diagram with strain similar to that observed for quenched HDPE elongated at room temperature, implying that the thermal stability of the crystal blocks composing the lamellae is only dependent on the crystallization temperature. The strain at a characteristic transition point associated with the first indication for the occurrence of a fibrillar structure remains essentially constant in spite of the large changes in drawing temperature and crystalline thickness. In addition, WAXS experiments were used to probe the texture changes accompanying the uniaxial elongation and yield the relationship between the orientational order parameters associated with the crystallites and the amorphous chain segments, and the imposed strain. The results support the existence of intralamellar slip processes from the very beginning of tensile deformation.

1. Introduction

Many polymers normally crystallize only to a certain extent – typically between 10% and 50%. This incomplete crystallization is due to the kinetic hindrance of entanglements between the polymeric chains that cannot be removed but are just shifted into the amorphous layers during solidification from the melt. This constraint leads to the formation of periodically stacked lamellar crystals with a periodicity of typically 10–50 nm and entangled amorphous polymeric chains in between forming the so-called semicrystalline state [1]. Being composed of alternating lamellar crystallites and amorphous polymeric phase, semicrystalline polymers always show a complicated deformational behavior when strained in the solid state. In order to obtain a detailed understanding of the molecular mechanisms contributing to the deformation of crystalline polymers, high-density polyethylene (HDPE) has always been chosen as a model polymer material because it is the simplest polymer with respect to its chemical structure and is used in a wide range of applications in daily life where mechanical stability is essential [2–7]. When being cooled from the quiescent melt, spherulites made up from stacks of crystallite lamellae having a thickness of several to tens of nanometers are usually observed in PE [1]. The hard crystalline phase provides rigidity to the system whereas the soft amorphous phase provides toughness to the material [8,9]. To a large extent, the mechanical properties of HDPE depend on its microstructure and morphology [10–15]. Typically,

* Corresponding author. Tel.: +86 431 85262907; fax: +86 431 85262954.
E-mail address: men@ciac.jl.cn (Y. Men).

0032-3861/$ – see front matter © 2009 Elsevier Ltd. All rights reserved.
doi:10.1016/j.polymer.2009.06.063

solid PE can be elongated to more than 400% in uniaxial extension [16,17]. As a consequence of tensile deformation, the original lamellar microstructure of PE is transformed into a fibrillar one where polymeric chains are preferentially oriented along the stretching direction [4,16–19]. However, a generally accepted picture of this lamellar to fibrillar transition accompanying the drawing process has not yet been evolved. It is essential to probe the micro-structural changes during mechanical deformation of the material in order to gain more insight into the molecular mechanisms of deformation being active in initially unoriented PE – thus providing possible routes for improvement of the material [20–28]. To account for the transformation of the spherulitic into the highly oriented fibrillar morphology, two general but distinctly different arguments have been proposed in literature dealing with the mechanical properties of PE. First, it is suggested that the deformation is accomplished by slips within the lamellae including crystallographic fine slips and intralamellar mosaic block slips [2,4,5,7,29–31]; second, stress-induced melting and recrystallization was proposed to be responsible for the variation of morphology in the deformation process [32–35]. Experimental evidence for both arguments have been extensively reported including microscopic and X-ray diffraction investigations supporting the slip mechanism [2,6,7] and small-angle X-ray scattering (SAXS) experiments favouring the melting–recrystallization scheme [36–38].

In recent years, many investigations based on "true stress–strain" experiments reveal that a combination of the two processes discussed above is activated in the course of tensile deformation of semicrystalline polymers [8,26,39]. Upon stretching, block slippage within the crystalline lamellae takes place first, followed by the stress-induced fragmentation and recrystallization of the freed polymeric chains at a strain larger than the yield strain. It was also found that the onset of the stress-induced fragmentation and recrystallization process depends on the interplay between the entanglement state of the amorphous phase and the stability of the crystalline blocks [9]. In the case of PE, a critical "true" strain of about 0.6 for this onset point was obtained irrespective of crystallinity, temperature, and strain rate, as well as crystalline lamellar thickness [39]. On the one hand, the evolution of the microstructure from the originally macroscopically isotropic semicrystalline polymer to a highly oriented fibrous material induced by the tensile deformation was assumed to proceed via fragmentation and recrystallization and can be evidenced directly with the SAXS technique in the bulk state without special sample preparation procedures [20,22,40–42]. On the other hand, it has been postulated that this process can be explained on the ground of crystallographic mechanisms alone [7,31,43,44]. According to this approach the plastic deformation initially proceeds primarily by fine chain slip, which leads to reorientation of both chain direction and lamella normal and, consequently, substantial thinning of lamellae and reduction of the long period. Such thinning leads to slip instabilities and then to heavy fragmentation of lamellae into small crystalline blocks. Now, these blocks become free of constraints imposed previously upon the lamellae and can not only rotate to produce a new long period along the drawing direction but also reshape to reduce the interfacial energy. The latter effect leads to an increase in the thickness of the lamellae thinned in the previous step to a value that is characteristic for the actual temperature.

The drawing temperature is expected to strongly affect the deformation behavior on the microscopic and macroscopic scale, because many of the deformation mechanisms operative in the semicrystalline polymers are temperature dependent [6,45–47]. As pointed out in literature, both crystallographic deformation via rearrangement of the crystalline blocks and stress-induced fragmentation and recrystallization should be enhanced when raising the tensile deformation temperature [48–51]. In fact, one often meets situations where a product made from polymers is used under varying temperature conditions in real-life applications. Moreover, many procedures used in industry to determine the lifetime of the final products are conducted at elevated temperatures in order to reduce testing time [52]. In such cases, knowledge about the changes of microstructure occurring in the deformational process upon stretching at different temperatures is indispensable. Although real-time in situ deformation experiments can eliminate the effect of sample relaxation and thereby allowing accurate information about the microstructure to be recorded, it is experimentally difficult and thus cannot provide the full picture dealing with the lamellar to fibrillar transition occurring in the necking process due to limited time resolution of most of available set-ups and the rapid irregular change in strain rate in the shoulder of the necking sample. However, by taking advantage of scanning experiments subsequent to tensile deformation it is possible to identify the complete process of morphological changes and set the basis for the theoretical understanding of the mechanisms and laws controlling deformation in polymeric solids.

In the present work, we study the micro-structural evolution of HDPE at different deformation ratios after stretching at different temperatures by means of positional scanning synchrotron SAXS and wide-angle X-ray scattering (WAXS). As will be presented in the following, SAXS results first of all confirm the occurrence of both deformation mechanisms discussed above: a transition from mosaic block-slip processes to fragmentation and recrystallization at a certain strain is deduced from 2-D SAXS patterns. It is also found that the thermal stability of the crystalline blocks after coarse slip is only crystallization temperature dependent. Furthermore, the strain at a characteristic transition point associated with the onset of the formation of fibrils turns out to be essentially constant, independent of drawing temperature and thickness of the crystalline lamellae. This work therefore provides micro-structural insight of the previous established understanding on the deformation mechanism. It must be stressed that the data treatment is performed in a semiquantitative manner, mainly relying on the interpretation of changes observed in the scattering patterns upon variation of the experimental parameters, including temperature of drawing, strain, as well as initial morphology. No effort is undertaken to give a complete description of the data by fitting a structural model to the data, because still too many structural details of the material are not well enough known; when stretching semicrystalline samples, the original structure deforms, fragments and in some cases starts to melt, whereas at the same time new structural features appear due to the reorganisation of the free polymer chain segments. Furthermore, as will be discussed below no unique data treatment for the whole set of samples was possible due to changes in the symmetry of the material.

2. Experimental section

The HDPE used in this study was supplied by BASELL Polyolefine, Frankfurt, Germany. The molecular weights were $M_w = 3.24 \times 10^5$ g/mol and $M_n = 2.3 \times 10^4$ g/mol. The material was first compression molded at 180 °C and held in the molten state for 5 min to relieve any orientation developed. Solidification was induced by rapidly quenching the melt into ice water yielding a plate of 2 mm thickness. Samples prepared in this way were deformed without strain-whitening at each temperature used in this work. Such a strain-whitening normally occurs for HDPE samples prepared by slowly cooling down from the molten state when the samples were stretched at room temperature. Strain-whitening indicates the occurrence of cavitations in the samples during deformation which will spoil SAXS patterns due to the much enhanced contrast between the cavitations and surrounding polymeric matrix [53]. In

the preparation of the isothermally crystallized specimen, the molten sheet was quickly transferred to a thermostated oil bath, which had been preset at a crystallization temperature of 125 °C. After isothermal crystallization for 24 h, the sample obtained was used to carry out the deformation experiment. Rectangular strips of 20×70 mm^2 dimension were cut from the plates and mounted on a stretching device in a heating chamber. When the desired temperature in the heating chamber was constant for 5 min, the strips were stretched at given temperatures (23, 80, 100 and 120 °C) until neck propagation over a large portion of the sample at a constant crosshead speed of 10 mm/min occurred. The isothermally crystallized sample was only stretched at 120 °C to avoid strain-whitening as mentioned above. The drawn samples were not fixed at their two ends in the stretched state when being taking out of the tensile machine. In order to measure the strain of the sample along the neck shoulder accurately, optical images of the samples were employed. Assuming a constant volume during the stretching, the Hencky measure of the strain ε_H was used as a measure for the deformation which is defined as

$$\varepsilon_H = 2 \ln \frac{b_0}{b} \quad (1)$$

where b_0 and b represent the widths of the undeformed and the deformed area located at certain spots on the samples.

Synchrotron SAXS measurements were performed at the beamline BW4 at HASYLAB, DESY, Hamburg, Germany. The energy

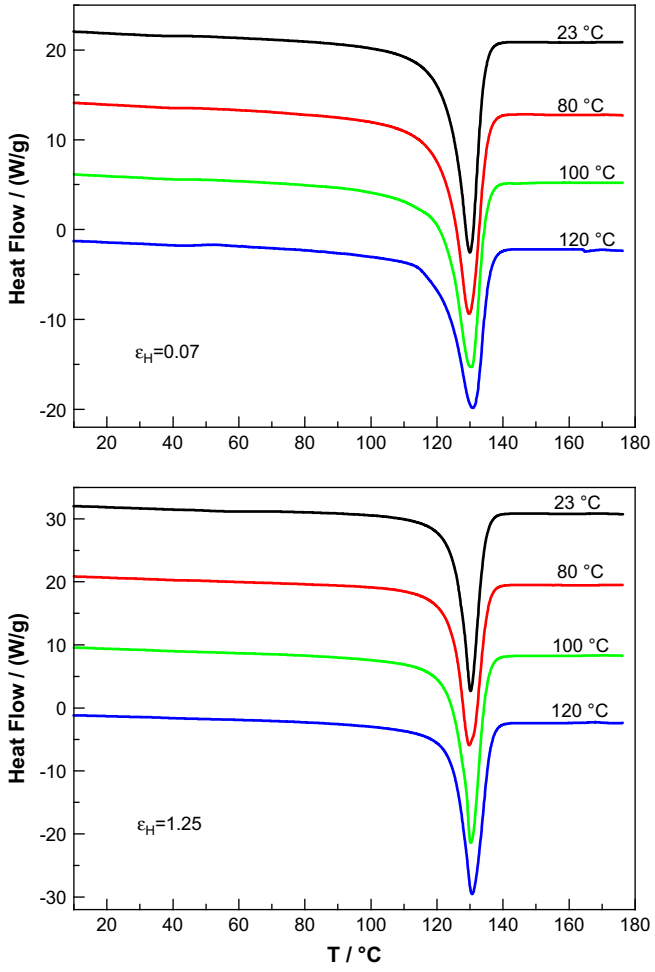

Fig. 1. DSC melting thermograms: samples in the un-necked region (top) and in the necked zone (bottom) after stretching at 23, 80, 100 and 120 °C. Curves were shifted vertically for the sake of clarity. Heating rate is 10 K/min.

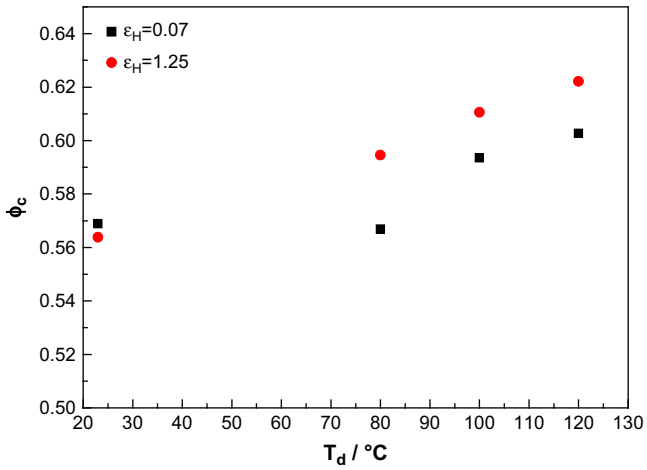

Fig. 2. Variation of the degree of crystallinity measured for samples in un-necked and necked zones with the stretching temperature.

of the X-ray radiation was 8.979 keV, resulting in a wavelength of 0.13808 nm. The size of the primary X-ray beam at the sample position was 0.4×0.4 mm^2. The pre-stretched sample was mounted onto a 2-dimensional translational stage at the beamline at a sample to detector distance of 6987 mm. At this distance the effective scattering vector q ($q = (4\pi/\lambda)\sin\theta$, where 2θ is the scattering angle and λ the wavelength) range is 0.03–0.55 nm^{-1}. The primary X-ray beam was first positioned at the middle of the horizontally placed sample bar. The samples were then moved stepwise in such a way that the X-ray beam scanned over the neck shoulder at a step length of 0.5 mm thus covering the stretching ratio from 0.07 up to 1.30 on a single sample. SAXS patterns were collected at every step within 120 s. The SAXS data were calibrated for background scattering and normalized with respect to the primary beam intensity. Changes in scattering intensities due to varying sample thicknesses have been corrected for by measuring sample adsorption using ionization chambers before and after the sample and performing the respective data correction.

WAXS experiments were carried out in order to determine the crystal texture changes and orientation of amorphous chains of the deformed samples as a function of the imposed strain. Synchrotron WAXS measurements of this set of stretched samples were performed at BSRF, Beijing, China with the wavelength of X-ray being 0.154 nm. Each WAXS diagram obtained in the center of the sample neck was collected within minutes at a sample to detector distance of 234 mm.

In order to gain more information about the samples subjected to different tensile deformation ratios, differential scanning calorimetry (DSC) measurements were conducted on deformed samples at two extreme draw ratios. A DSC 2920 (TA Instruments) was used during the experiments with a heating rate of 10 K/min. The melting point T_m denotes the minimum of the thermograms during heating. The crystallinity is derived from integrating the DSC traces with respect to a baseline drawn as a tangent to the trace at 40 and 150 °C and relating the derived heat to the melting enthalpy of hypothetical 100% crystalline polyethylene of 293 J/g [54].

3. Results and discussion

3.1. DSC results

Before considering the structural evolution registered by SAXS patterns, we present the results from thermal analysis on the HDPE samples in order to check the influence of tensile deformation and

drawing temperature on the degree of crystallinity. Fig. 1 shows DSC melting curves of samples of un-necked parts and in the neck zones after having been deformed at elevated temperatures. Because the plastic deformation set in already before the yield point, the un-necked region of the samples exhibited also several percents of permanent deformation [55,56]. The values of the true strain indicated on the plots of Fig. 1 were obtained using Equation (1). As is seen deforming at different temperatures hardly affects the melting point of the specimens, which may be due to the occurrence of melting and recrystallization process accompanying the heating scans. The values of crystallinity under different conditions are compiled in Fig. 2. Two different kinds of behavior were observed for the two types of samples. When stretching at room temperature, the crystallinity of the necked sample decreases slightly as compared to the un-necked one; this effect is ascribed to the destruction of original lamellar crystallites and formation of defective crystals during deformation. The crystallinities of both samples exhibit different tendencies after drawing at elevated temperatures. The crystallinity of the samples in the un-necked zone remains essentially unaffected when the drawing temperature is lower than 80 °C. It increased slightly for the sample elongated at 120 °C. This increase is due to the thickening and perfectioning of the existing crystalline lamellae of the quench-crystallized samples during stretching at elevated temperatures. It is likely that the samples stopped crystallizing during quenching at a temperature higher than 80 °C. However, for the samples in the necked zone, a continuous increase in the crystallinity with increasing temperature is observed. This is because more perfect crystallites can be generated during mechanical drawing at higher deformation temperatures. The crystallinity for the samples in the necked zone reaches values about 2% larger than those of the un-necked region after being stretched at elevated temperatures in the range from 80 to 120 °C. This is due to the fact that preferential orientation of the crystalline lamellae and polymeric chains in the necked zones facilitates the perfectioning and thickening of the crystallites leading to a higher degree of crystallinity as compared to the un-necked regions.

3.2. SAXS results

To elucidate the textural variations on the lamellar length scales during deformation, selected SAXS patterns for quenched HDPE samples stretched at different temperatures are presented as a function of the indicated imposed strains in Fig. 3. The SAXS patterns for the periodic lamellar structure of HDPE exhibit maxima

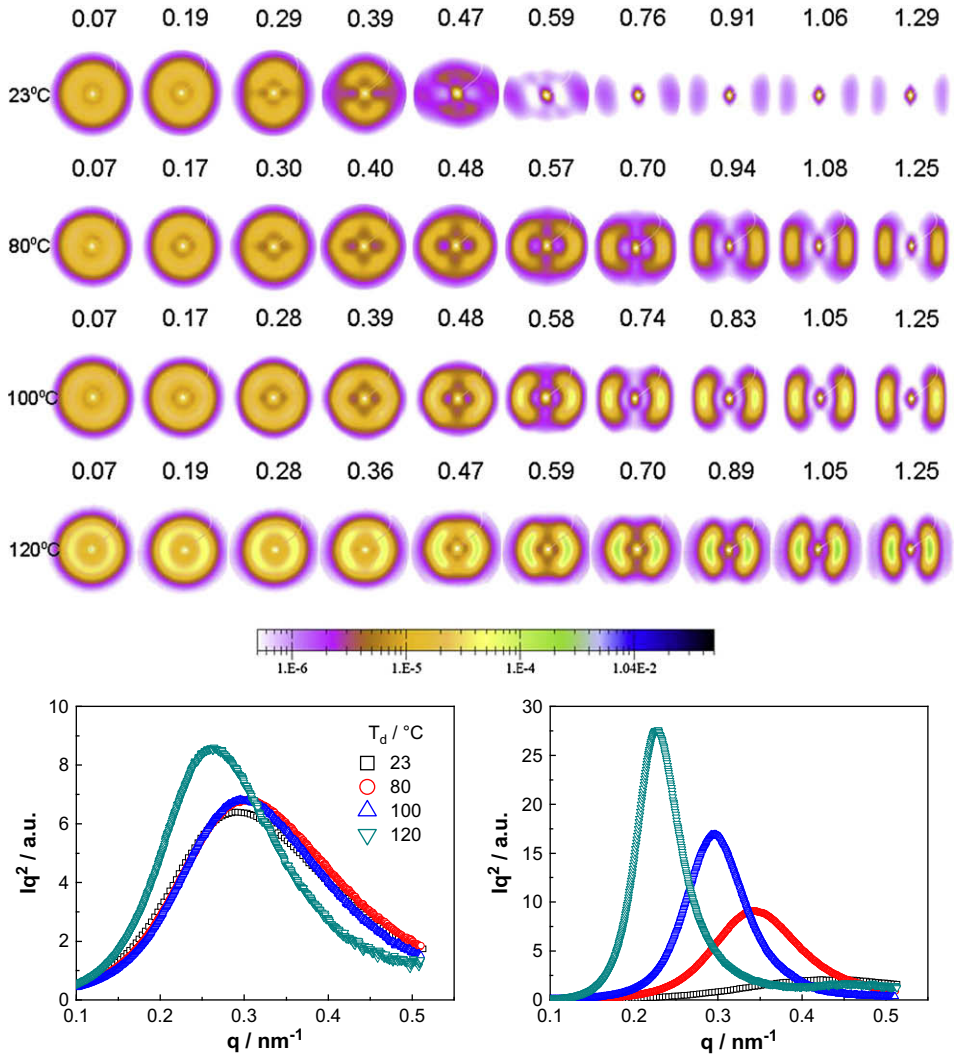

Fig. 3. Selected small-angle X-ray scattering patterns of quenched HDPE uniaxially drawn at 23, 80, 100, and 120 °C (from top to bottom) taken at different imposed strains as indicated on the graph. Stretching direction is horizontal. For a better visualization of the changes in scattering intensity after annealing and deformation, plots including the one-dimensional scattering intensity distributions of the samples at strains of 0.07 (left) and 1.25 (right) were given in the bottom.

at q_{max} when scanning along certain directions. The value of the long spacing (d_{ac}) can be calculated using the Bragg equation:

$$d_{ac} = \frac{2\pi}{q_{max}} \quad (2)$$

The long spacing d_{ac} is defined as the average thickness of a lamella together with one interlamellar amorphous layer measured along the lamella normal. At this point of data treatment we do not take any symmetry considerations into account that might necessitate

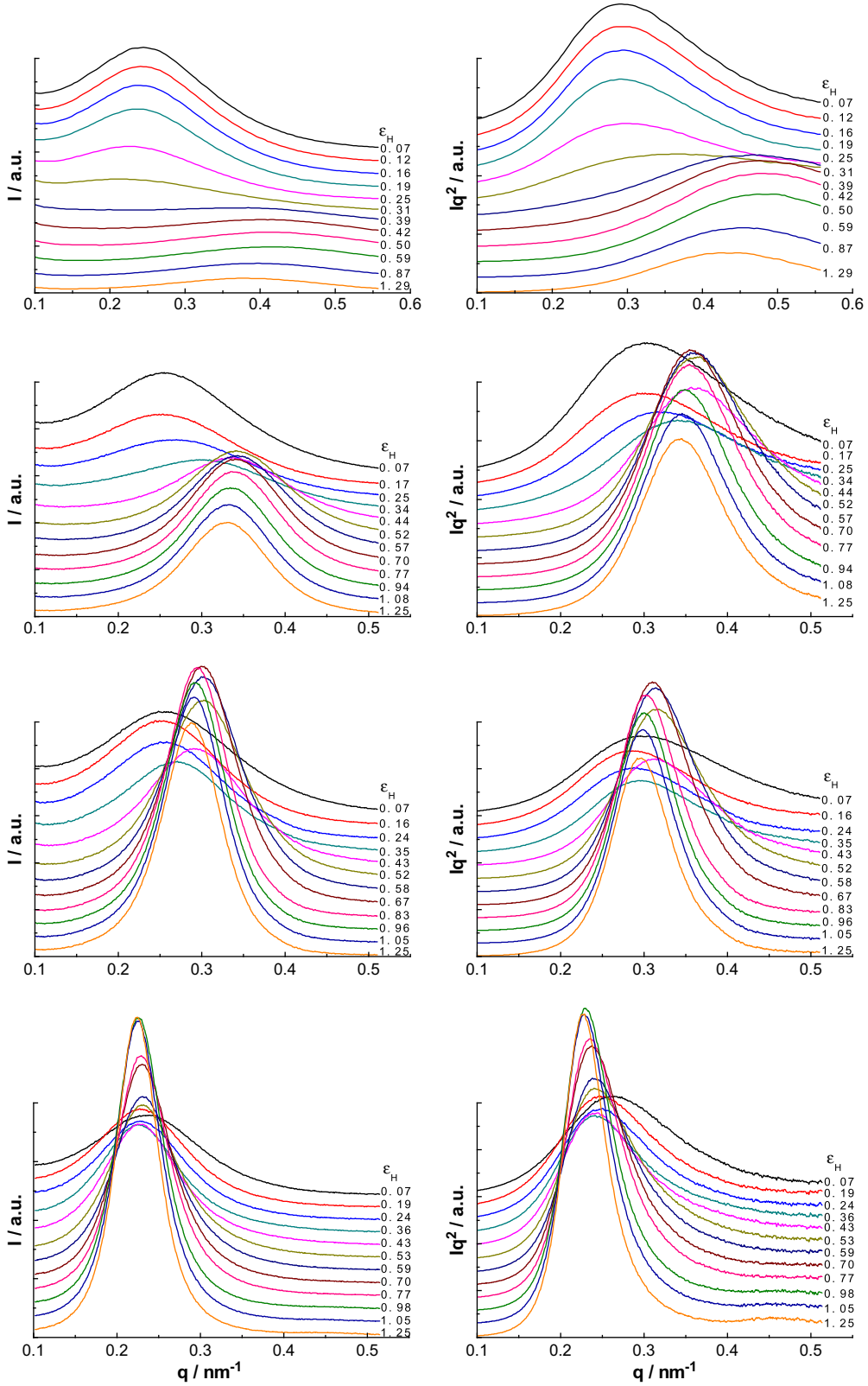

Fig. 4. SAXS: one-dimensional scattering intensity distribution profiles without Lorentz correction (left) and with Lorentz correction (right) taken along the stretching direction at different deformations for samples uniaxially stretched at 23, 80, 100 and 120 °C (from top to bottom). Peak positions were used to calculate the long periods (d_{ac}).

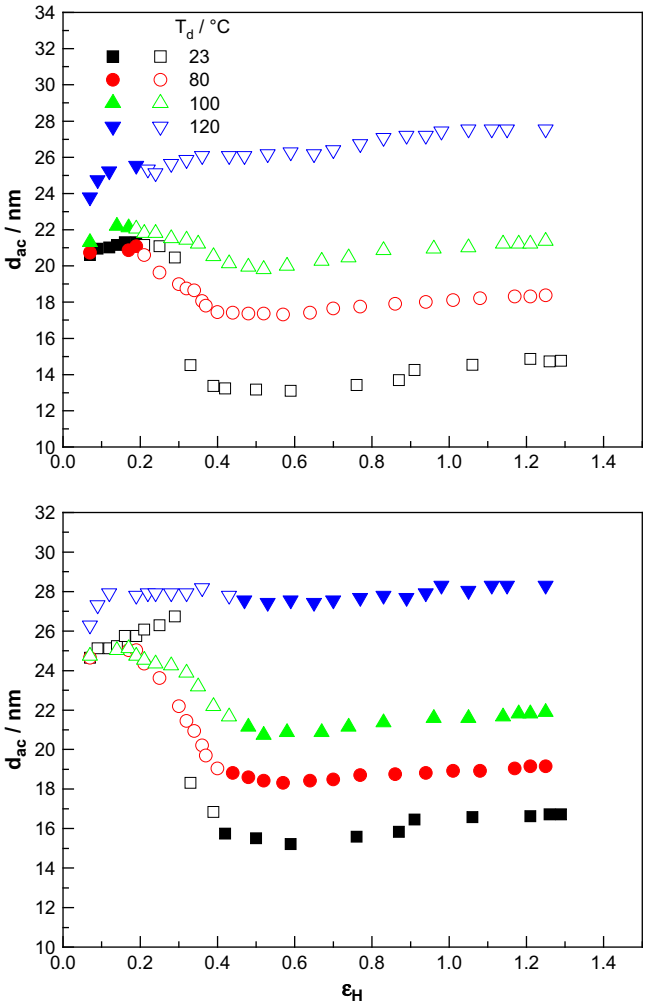

Fig. 5. True-strain dependence of the long spacing d_{ac} along the drawing direction after stretching at elevated stretching temperatures. Top: Data derived from Lorentz-corrected scattering curves; filled symbols represent regions where Lorentz correction is sure to apply. Bottom: Data evaluated from scattering curves without Lorentz correction; filled symbols stand for regions where anisotropy is high enough such that no Lorentz correction must be applied.

the multiplication of the isotropic intensity values with q^2 (Lorentz correction). We are aware of the fact that this leads to an error when comparing the d_{ac} values from isotropic and highly oriented samples. This point will be addressed in more detail below. As mentioned above, the un-necked region exhibits a permanent macroscopic deformation of $\varepsilon_H = 0.07$ which is also evident from the slight anisotropy of the scattering patterns at this deformation. With increasing deformation the SAXS patterns become more anisotropic; finally a pattern with two straight streaks perpendicular to the stretching direction at high deformation ratios develops – indicating a highly oriented lamellar structure after deformation. Additionally, in the course of the transition from the original isotropic scattering distribution to highly anisotropic streak-like scattering patterns several characteristic features can be identified upon closer inspection of the SAXS data.

3.2.1. Quenched sample stretched at 23 °C

Stretching leads to a sequential change in SAXS pattern as follows: As the deformation ratio is increased, the SAXS patterns transform from a scattering pattern with peaks perpendicular to the stretching direction at low strains, and four-point scattering diagram at moderate strains, eventually to highly anisotropic scattering intensity distribution with two scattering peaks aligned in the meridional direction (i.e., along the stretching direction). Initially, the original scattering intensity in the meridian direction becomes weaker with increasing stretching ratio, indicating a loss of the positional correlation between the crystalline lamellae with their normal along the stretching direction. Meanwhile, a new meridian long spacing scattering peak appears gradually at larger q values corresponding to a reduction of the long period of the respective stacks of lamellae. This finding is in line with the previously proposed process of fragmentation and recrystallization during deformation: Since the deformation was imposed at room temperature, the recrystallization process produces lamellae that are thinner than the original ones because of the high undercooling with respect to the typical crystallization temperature of HDPE [57]. As far as the original lamellar crystallites are concerned, two main features can be identified from the SAXS diagrams. First, the scattering intensity decreases strongly with increasing deformation, implying that the original lamellar stacks are destroyed in the course of deformation. Second, a four-point SAXS pattern occurs at small strains ($\varepsilon_H = 0.47$), reflecting a shearing or tilting of the oriented lamellar crystallites. Upon further deformation, the positions of these peaks gradually move closer to the equator. These observations can be tentatively explained in the following way. First, lamellae with their normal parallel to the stretching direction are molten or broken into blocks with fragments losing their positional correlation because they cannot easily undergo slip-like deformation. This point was already addressed above. Second, lamellae with their normal perpendicular to the stretching direction are broken by external forces resulting in a loss of SAXS intensity in the equatorial direction. Third, lamellar stacks with their normal situated between the above two extremes are able to experience intralamellar slip, keeping some correlation within the stacks.

3.2.2. Quenched samples stretched at elevated temperatures

The effect of drawing temperature on the SAXS patterns and thus the microstructure of the HDPE samples is also derived from the data in Fig. 3. First, there is an overall increase in the scattering intensity after stretching at higher temperatures relative to that

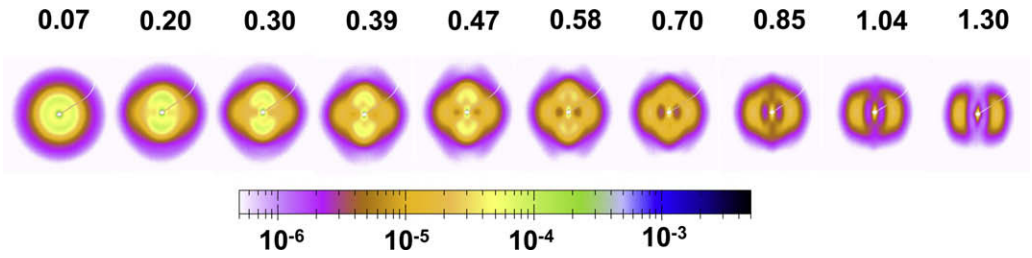

Fig. 6. Selected small-angle X-ray scattering patterns of isothermally crystallized HDPE uniaxially drawn at 120 °C taken at different strains as indicated on the graph. Stretching direction is horizontal.

measured for HDPE stretched at room temperature, which is evidence for the perfection of crystalline lamellae accompanied by an increase of the electron density difference between the crystalline lamellae and the amorphous layers in between. Second, the position of the maximum scattering intensity moved to smaller q values with increasing drawing temperature implying that the crystalline lamellar long spacing increased. However, at moderate deformations, several qualitative differences of the shape of the SAXS patterns were observed with respect to the drawing temperature (e.g. patterns at strains around 0.4). In addition, it must be noted that when stretching at elevated temperatures, the scattering intensity after deformation becomes stronger in comparison to that observed in the undeformed state. This effect may be attributed to an enhanced positional correlation between the highly oriented fiber structures composed of stacks of lamellae aligned along the drawing direction after mechanical deformation of specimens at higher temperatures.

In an effort to elucidate the evolution of the lamellar long spacing after deformation at elevated temperatures, the one-dimensional scattering intensity distributions along the stretching direction were considered, see Fig. 4. We took two approaches: in order to represent the data of the isotropic samples with the correct q weighting the scattering intensity was multiplied by q^2 for data processing (Lorentz correction) [58,59]. For the data with fiber symmetry, i.e., at high stretching ratios, no Lorentz correction was applied. Both sets of data are represented in Fig. 4. Obviously, both approaches are correct only for the respective extreme situations where the lamellar stacks are distributed isotropically, i.e., sample without strain, and stacks of lamellae perfectly oriented with their normal along the drawing direction. In between these extremes no unique recipe for data treatment can be given because of the uneven distribution of scattered intensity in reciprocal space. The long spacing values for samples after deformation at elevated temperatures measured along the stretching direction were obtained according to Equation (2) for both data sets in Fig. 4 and are given in Fig. 5. The data show that although the long spacings derived from Lorentz-corrected data at small strains exhibit a few nanometers difference from the respective long spacings calculated from the uncorrected data, it does not change the characteristic variation of the long spacing as a function of strain. This means that for a semiquantitative discussion of the dependence of the long spacing on strain the type of data treatment (Lorentz correction versus no correction) plays only a subordinate role. The variations of the long spacing values along the stretching direction with strain exhibit a transition-like behavior, as given in Fig. 5. For the sample stretched at room temperature, there exists a considerable drop in long spacing from about 21 nm before necking to around 15 nm in the necked zone. This behavior is assumed to be due to the fragmentation and recrystallization process, i.e., the lamellar stacks established after stretching form by taking up the polymer chain segments freed from destabilized original crystalline lamellae that have been destroyed during deformation. The transitional strain lies between 0.3 and 0.4; this is in accordance with previous results obtained using true stress–strain experiments [39]. A closer look reveals that the long spacing along the stretching direction increases slightly both before and after the transition zone. This can be interpreted by assuming that under external tensile stress in those lamellar stacks with their normal parallel to the stretching direction the interlamellar amorphous layers are stretched. Fig. 5 clearly shows that the long spacing of the oriented fiber structure along the drawing direction increases with increasing stretching temperature, although the initial long spacing of the specimens is found to be nearly constant for temperatures below 100 °C, indicating that the crystallization had been essentially completed above 100 °C but below 120 °C during the quenching process. This drawing temperature dependency of the long spacing of the highly oriented fibrillar system can be assuming that the original lamellar crystallites are destroyed through slippage followed by recrystallization processes at the corresponding temperature at which the tensile deformation takes place. When the drawing temperature is lower than 100 °C, the long spacing follows essentially the trend described above through the transitional strain zone where a strong decrease of the long spacing occurs which then remains almost constant in the late stages of deformation.

When the sample was stretched at 120 °C, in addition to the further increase of the long spacing as compared to that at lower stretching temperatures, one finds a distinctly different behavior in the change of the long spacing with strain. Instead of strong decrease in the transitional strain region, the long spacing increases by around 2 nm relative to that measured in the initial undeformed state. This supports the statement that crystallization is completed below 120 °C in the preparation of the specimens. With further increase of the deformation ratio, the long spacing increases slightly. This behavior is due to the fact that the drawing temperature is higher than the crystallization temperature in the production of HDPE specimen and the resulting structure is determined solely by the temperature at which the deformation is carried out as a consequence of recrystallization. More insight can be extracted from the 2-dimensional SAXS patterns in Fig. 3. A similar sequence of SAXS patterns can be observed when the drawing temperature is below 100 °C. The four-point patterns of the original lamellar stacks,

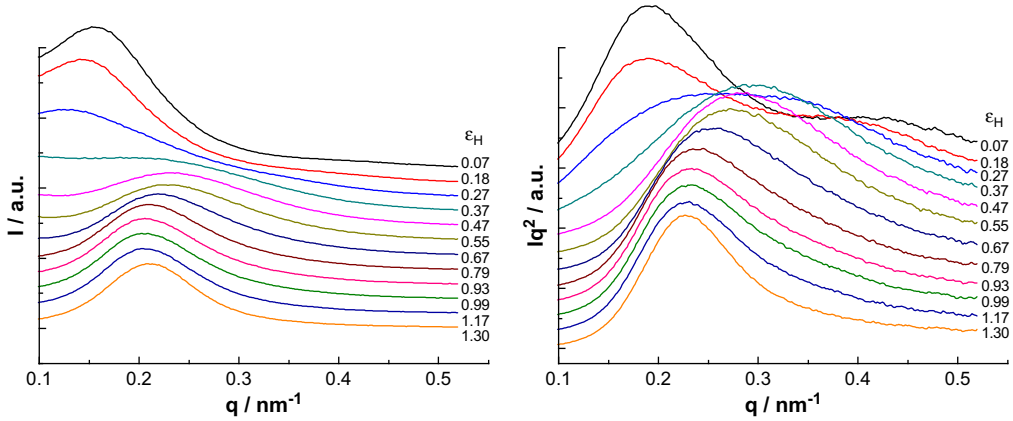

Fig. 7. SAXS: one-dimensional scattering intensity distribution profiles without Lorentz correction (left) and with Lorentz correction (right) taken along the stretching direction at different deformation ratios for the isothermally crystallized HDPE sample uniaxially stretched at 120 °C. Peak positions were used to calculate the long periods (d_{ac}).

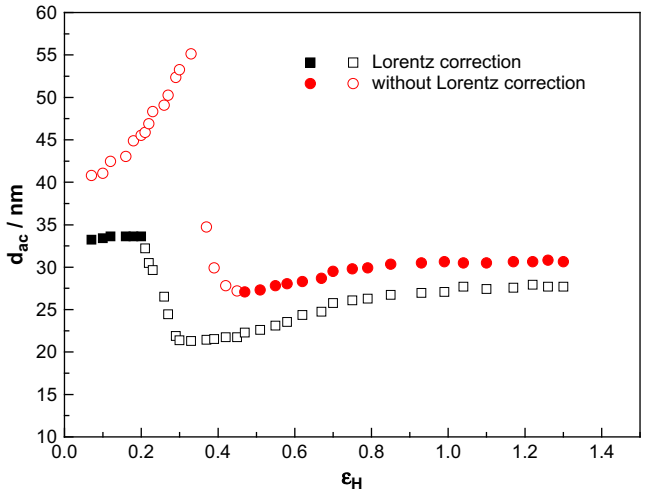

Fig. 8. True-strain dependence of the long period d_{ac} along the drawing direction at the stretching temperature of 120 °C measured for the isothermally crystallized HDPE.

compare data of 23 °C sample, are stable when stretching at 80 and 100 °C. As the drawing temperature is raised to 120 °C, the sheared crystalline blocks become unstable; they melt, also driven by intralamellar block-slip processes. Subsequently oriented recrystallization at the corresponding temperature occurs. As soon as the new lamellar stacks along the stretching direction – possessing larger long spacing and thicker lamellae than the original ones – have been formed at a strain of about 0.4, the original tilted lamellae melt and the freed polymers recrystallize – at least partially – onto the newly developed lamellae, leading to the appearance of highly anisotropic scattering patterns. Therefore, the physical origin of the two different micro-structural changes occurring with increasing strain as manifested by the SAXS patterns, mainly lies in the stability of crystal blocks composing the lamellar crystallites. When the crystallization temperature is higher than the temperature imposed during deformation, the crystalline blocks still remain stable, even if they undergo severe internal deformation. In contrast, if the crystallization temperature is lower than the applied drawing temperature, the crystal blocks become unstable, and melt and recrystallize at the corresponding temperature at which tensile drawing has been performed.

3.2.3. *Isothermally crystallized sample stretched at 120 °C*

In order to further understand the role played by structural features in the deformation process, the morphological development of deformed HDPE specimen isothermally crystallized at 125 °C was also probed and compared to the quenched sample stretched at the same temperature. Selected SAXS patterns for the isothermally crystallized sample elongated at 120 °C are plotted in Fig. 6 as a function of strain. As the deformation ratio is increased, the SAXS patterns transform from a scattering pattern with peaks perpendicular to the stretching direction at low strains, and four-point scattering diagram at moderate strains, eventually to highly anisotropic scattering intensity distribution with two scattering peaks aligned in the meridional direction (i.e., along the stretching direction). At the same time, the scattering intensity decreases gradually with increasing strain as a consequence of the destruction of original crystals and the creation of defective lamellar stacks at lower temperature. Obviously, the change of the scattering patterns for the isothermally crystallized specimen followed the same sequence as that observed for quenched sample stretched at room temperature, but distinctly different from that measured for quenched sample drawn at a temperature of 120 °C. The discrepancy between the patterns collected from two samples with different thermal history at the same drawing temperature is due to the fact that the crystalline blocks generated at high

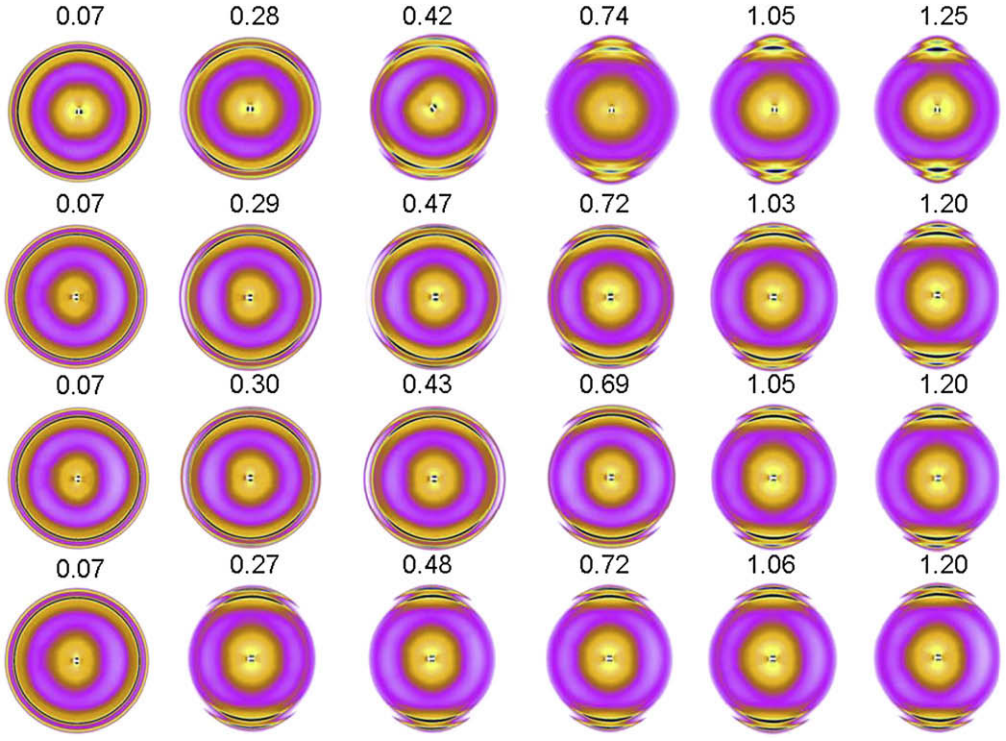

Fig. 9. Selected wide-angle X-ray scattering patterns of quenched HDPE, uniaxially drawn at 23, 80, 100, and 120 °C (from top to bottom) taken at different strains as indicated on the graph. Stretching direction is horizontal.

crystallization temperature (e.g. 125 °C) are thermally stable and can be preserved at intermediate strains when being stretched at 120 °C. This behavior is in accord with the polymer crystallization model devised by Strobl where the granular crystal blocks form first followed by the final lamellar crystallite via block merging in the growth of polymer crystallites [60]. Accordingly, although there is a profound influence of crystallization conditions on the general deformation characteristics of HDPE specimens, the molecular mechanisms underlying the lamellar to fibrillar transition are still invariant, involving a block-slip, fragmentation, and recrystallization sequence, independent of drawing temperature and crystallization temperature. Fig. 7 shows plots of the scattering intensity distributions along the drawing direction as a function of strain for the sample isothermally crystallized at 125 °C. Both sets of profiles including raw data and Lorentz-corrected data are presented. The resulting values of the long spacings for the sample after deformation are illustrated in Fig. 8. One observes a drop in the long spacing with increasing strain, which is similar to that found in quenched samples drawn at elevated temperatures with the exception of 120 °C. It must be noted that the strain associated with the onset of the formation of fibrils subsequent to the disaggregation of crystal blocks remains almost unchanged, being located at a true strain of about 0.4, when varying drawing temperature and crystalline thickness. This observation is consistent with the view of a block-like substructure of the lamellar crystallites as a basic feature for all melt-crystallized polymers [1]. Additionally, on detailed examination of the long spacing values derived from the two specimens deformed at 120 °C, it becomes clear that the resulting fibrillar structures show nearly the same value of the long spacing as samples drawn at the same temperature in spite of the large differences found in the initial isotropic state with respect to the long spacing, implying that the long spacing after deformation is independent of the microstructure of the initial sample, which is in good agreement with the assumption of deformation via fragmentation and recrystallization.

3.3. *WAXS results*

WAXS experiments were performed in order to explore changes with respect to texture by determining the degree of orientation of the crystals and the amorphous halo induced by uniaxial drawing. The discussion is based upon analysis of the azimuthal intensity distributions along the scattering circles. Sequences of WAXS patterns for quenched HDPE samples stretched at elevated temperatures are presented in Fig. 9. During the tensile drawing a considerable amount of the orthorhombic crystallites survived; only at high deformations an additional reflection developed, identified as originating from the metastable monoclinic phase [61,62]. The two Debye rings in the isotropic WAXS pattern are assigned to the 110- (inner circle) and the 200- (outer circle) lattice planes respectively. It can be seen that the crystallite orientation is a function of the strain. For all samples elongated the orthorhombic 200-reflection moved toward the equator first and broad maxima developed, followed by the orthorhombic 110-reflection at an oblique angle characterized by the presence of four-point patterns at low elongations. As the deformation proceeded, sharp maxima for both reflections were observed to be located on the equator and the azimuthal widths of the arcs gradually decreased. Note that no indication for the formation of an intensity maximum on the meridian can be detected, implying the occurrence of the coarse slips of the crystalline blocks at low deformations [39]. To obtain the precise azimuthal intensity distribution of the amorphous halo, the equatorial scans of the intensity distribution were derived from the WAXS patterns covering the scattering angle in the range of 5–30°, and a decomposition was carried out on the basis of Lorentzian functions. It was found that the position of the intensity maximum arising from the amorphous phase lies in the scattering angle range $19° < 2\theta < 20°$, which can well be discriminated from the 110-lattice plane scattering. Therefore, besides the orientation of lamellar crystallites, the orientation of the amorphous molecular chains can also be derived from WAXS measurements [63]. Fig. 10 depicts, as a typical result, the azimuthal scans of the intensity distribution of the orthorhombic 110- and 200-reflections, as well as the amorphous halo measured for the quenched specimen stretched at room temperature. Only one half of the data is presented for the sake of clarity. Deforming the sample, the scattering intensities of the 110-reflections and the amorphous halo split into four maxima and then narrow down toward the equator.

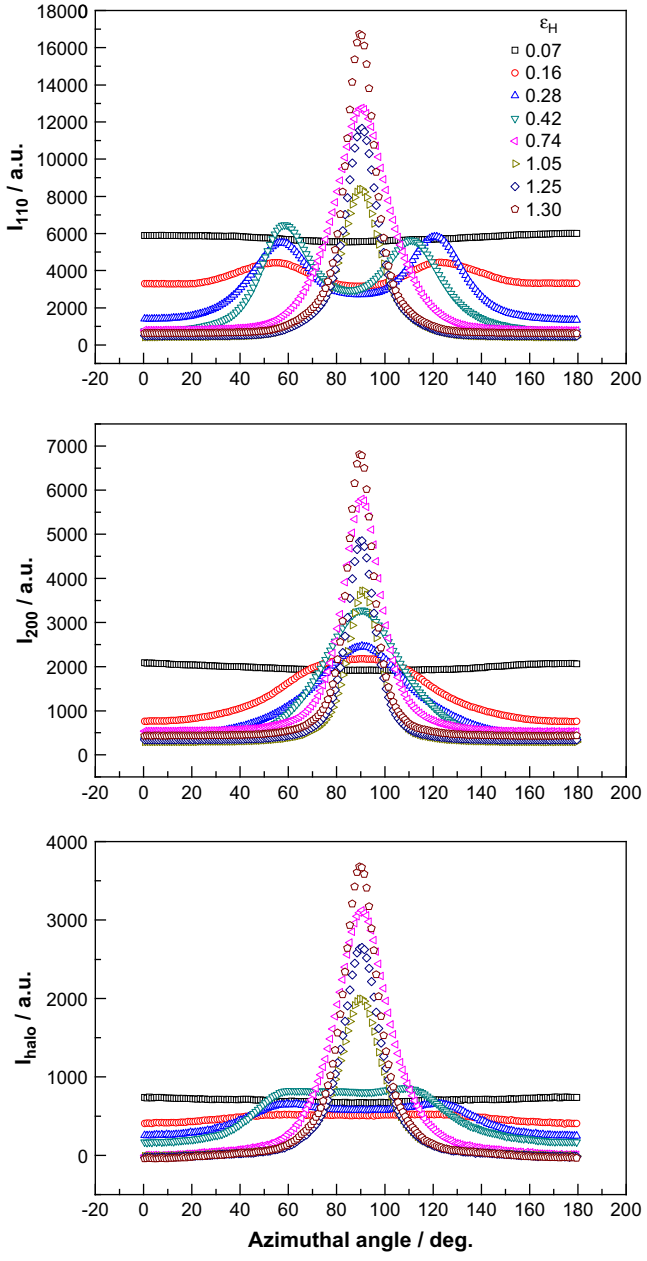

Fig. 10. Azimuthal intensity distribution of the 110-reflection (top), the 200-reflection (middle), and of the amorphous halo (bottom) measured for the quenched HDPE sample that was uniaxially drawn at room temperature as a function of the imposed strains.

The values of the degree of orientation associated with the lattice planes *hkl* and the amorphous halo can be derived from the azimuthal intensity distribution functions $I(\mu)$ along the respective circles by use of the Polanyi equation [64]:

$$\cos\vartheta_{hkl} = \cos\theta_{hkl}\cos\mu \tag{3}$$

where θ_{hkl} denotes the Bragg scattering angle. The equation correlates the azimuthal angle μ along the Debye circle with the angle ϑ_{hkl} between the extensional direction and the normal vector of the lattice plane. In the case of the amorphous halo, ϑ_{hkl} denotes the angle between the stretching direction and a vector perpendicular to the local direction of the amorphous chain. A measure for the degree of orientation in uniaxially oriented samples is the orientational order parameter proposed by Hermanns [65]. It is expressed as follows

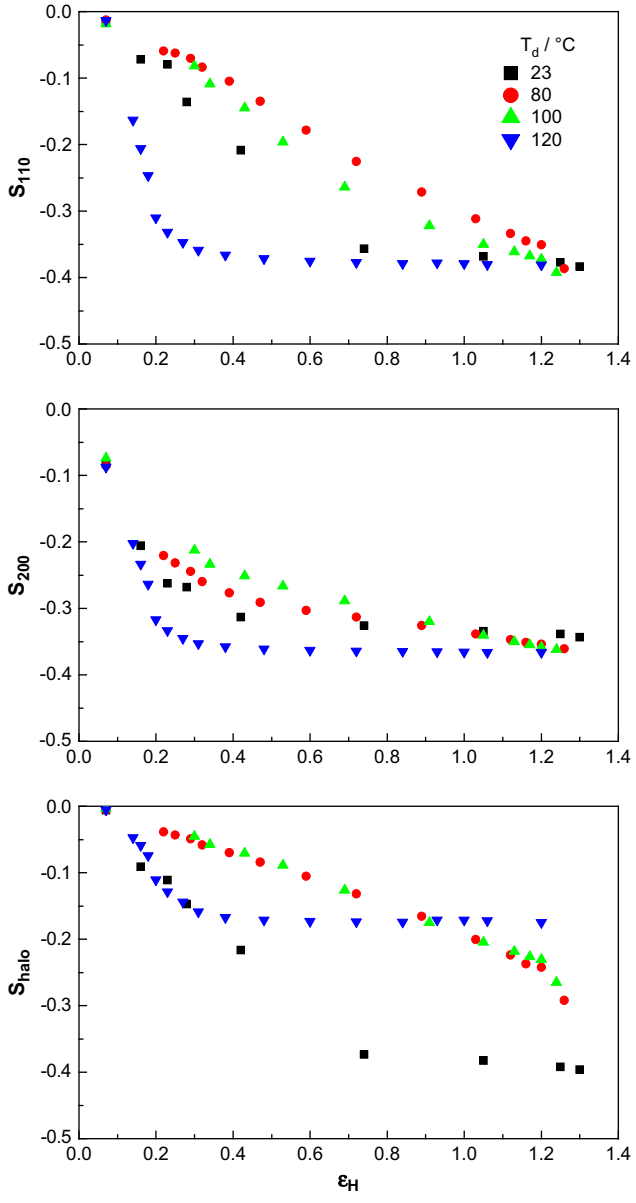

Fig. 11. Evolution of the orientational order parameters associated with the 110-reflection (top), the 200-reflection (middle), and the amorphous halo (bottom) as a function of the imposed strains measured for the quenched HDPE uniaxially stretched at 23, 80, 100, and 120 °C.

$$S_{hkl} = \frac{3\langle\cos^2\vartheta_{hkl}\rangle - 1}{2} \tag{4}$$

For the calculation of the degree of orientation of the amorphous halo, only ϑ_{halo} is used instead of ϑ_{hkl}. Note that the orientational order parameter in the present case assumes values in the range $-0.5 \le S \le 0$. For a perfect orientation of the lattice planes with their normal perpendicular to the stretching direction, the order parameter would be $S = -0.5$, while for an isotropic sample in the randomly oriented state, the order parameter becomes $S = 0$. Usually, the degree of orientation lies between the above two limiting values. The results for the orientational order parameters of the 110- and 200-reflections together with the amorphous halo are plotted as a function of strain in Fig. 11. For the samples stretched below 100 °C, the values for S_{110} and S_{200} decrease first rather strongly and later slowly with increasing strain. Particularly, the orientation of the 200-reflection changes more rapidly than the 110-reflection. On detailed inspection of the orientational order parameters associated with the crystal reflections as a function of strain, it becomes obvious that the degree of orientation of the crystallites is slightly larger for the sample deformed at room temperature, while the orientational order parameters of the lattice planes measured for the samples after uniaxial elongation at 80 and 100 °C behave similarly. This observation is explained by the fact that 80 °C is above the mechanical α relaxation temperature of HDPE [66–68]. The activation of the mechanical α process promotes additional relaxation of the orientation of the crystallites for HDPE samples elongated at higher temperatures. The change of the orientation of the amorphous molecular chain with strain is similar to that of the lamellar crystallites. The only difference between the two components is the somewhat lower degree of the orientation of the amorphous chains segments at all strains as compared to the orientation of the crystallites. When deforming the sample at a temperature of 120 °C one observes a distinctly different behavior for the strain dependencies of S_{110}, S_{200}, and S_{halo}. The orientational order parameters first exhibits a sharp drop, and then reaches a plateau starting at a strain of around 0.4, i.e., at a strain where fibril formation sets in. This is again evidence for the melting of the sheared lamellar crystallites and recrystallization leading to lamellar crystals with polymeric chains preferentially oriented along the stretching direction. One notes that the orientation of the amorphous segments under uniaxial drawing at high temperatures is markedly lower than the degree of orientation of the crystallites; this is attributed again to the activation of the mechanical α process leading to an extensive relaxation of the highly stretched amorphous chain segments located between crystalline lamellae [63,69].

4. Conclusions

Our scanning synchrotron SAXS experiments support previous evidence for the deformation mechanism of semicrystalline polymers based on stress-induced fragmentation and recrystallization processes occurring at a certain strain. Additionally, the effect of drawing temperature on quenched samples deformed to different strains was investigated. It was found that a common sequence of deformation processes is active in samples elongated below 100 °C, whereas deforming the sample at the temperature of 120 °C yields a peculiar deformation feature. Under the action of the imposed strain the original lamellar crystallites melt and recrystallize at 120 °C induced by intralamellar block-slip processes; the new crystal blocks form with their normal parallel to the stretching direction. They exhibit a larger long period. The deformation behavior of the sample isothermally crystallized at 125 °C and deformed at 120 °C is similar to the one of the quenched sample

stretched at room temperature. Hence, it is concluded that the thermal stability of the crystalline blocks is only crystallization temperature dependent. The critical strain value where fibrils show up for the first time and crystal blocks no longer can be assigned to individual lamellae coincides for all samples studied (at a value of about 0.4) in spite of the large variations in the drawing temperature and crystalline thickness. As it turns out, a one-to-one correspondence between the long spacing of the resulting fibrillar structure and the drawing temperature exists, regardless of the initial morphology. Using WAXS measurements both the orientation of the crystallites and the degree of orientation of the amorphous chain segments was determined. The strain dependencies of S_{110}, S_{200}, and S_{halo} reveal that the orientation of all structural components is greater for the sample stretched at room temperature as compared with those elongated below 100 °C. This difference is due to the activation of the mechanical α relaxation process at high temperatures. When the sample was uniaxially elongated at 120 °C, the orientational order parameters drop with increasing strain and remain almost constant commencing at a strain of about 0.4. This is in agreement with a model where sheared lamellar crystallites melt, with subsequent oriented recrystallization.

Acknowledgment

Y.M. thanks the "Hundred Talents Project" of the Chinese Academy of Sciences, the National Basic Research Program of China (2005CB623800), National Natural Science Foundation of China (50603024 and 50621302) and HASYLAB project II-20052011. We thank R. Döhrmann and M. Dommach for assistance in SAXS experiments at HASYLAB.

References

[1] Strobl G. The physics of polymers. Berlin: Springer; 1997.
[2] Bowden PB, Young RJ. J Mater Sci 1974;9:2034.
[3] Hay I, Keller A. Kolloid Z Z Polym 1965;204:43.
[4] Peterlin A. J Mater Sci 1971;6:490.
[5] Young RJ, Bowden PB, Ritchie JM, Rider JG. J Mater Sci 1973;8:23.
[6] Keller A, Pope DP. J Mater Sci 1971;6:453.
[7] Schultz J. Polymer materials science. New Jersey, Englewood Cliffs: Prentice-Hall; 1974.
[8] Men Y, Strobl G. J Macromol Sci Phys 2001;B40:775.
[9] Men YF, Rieger J, Strobl G. Phys Rev Lett 2003;91:095502.
[10] Bartczak Z. Macromolecules 2005;38:7702.
[11] Failla MD, Mandelkern L. Macromolecules 1993;26:7167.
[12] Kennedy MA, Peacock AJ, Mandelkern L. Macromolecules 1994;27:5297.
[13] Kiass N, Khelif R, Boulanouar L, Chaoui K. J Appl Polym Sci 2005;97:272.
[14] Yang L, Niu Y, Wang H, Wang Z. Polymer 2009;50:627.
[15] Jauffres D, Lame O, Vigier G, Dore F. Polymer 2007;48:6374.
[16] Lin L, Argon A. J Mater Sci 1994;29:294.
[17] Ward I. Mechanical properties of solid polymers. New York: Wiley; 1983.
[18] Men Y, Strobl G. Macromolecules 2003;36:1889.
[19] Men YF, Rieger J, Lindner P, Enderle HF, Lilge D, Kristen M, et al. Polymer 2007;48:2464.
[20] Butler MF, Donald AM, Bras W, Mant GR, Derbyshire GE, Ryan AJ. Macromolecules 1995;28:6383.
[21] Hughes DJ, Mahendrasingam A, Heeley EL, Oatway WB, Martin C, Towns-Andrews E, et al. J Synchrotron Radiat 1996;3:84.
[22] Jiang ZY, Tang YJ, Men YF, Enderle H, Lilge D, Roth SV, et al. Macromolecules 2007;40:7263.
[23] Pawlak A, Galeski A. Macromolecules 2005;38:9688.
[24] Ran SF, Wang ZG, Burger C, Chu B, Hsiao BS. Macromolecules 2002;35:10102.
[25] Tang YJ, Jiang ZY, Men YF, An LJ, Enderle H, Lilge D, et al. Polymer 2007;48:5125.
[26] Men Y, Strobl G. Chin J Polym Sci 2002;20:161.
[27] Young P, Stein RS, Kyu T. J Polym Sci Polym Phys 1990;28:1791.
[28] Song HH, Argon AS, Cohen RE. Macromolecules 1990;23:870.
[29] Bartczak Z, Lezak E. Polymer 2005;46:6050.
[30] Seguela R, Rietsch F. J Mater Sci Lett 1990;9:46.
[31] Galeski A, Bartczak Z, Argon AS, Cohen RE. Macromolecules 1992;25:5705.
[32] Flory PJ, Yoon DY. Nature 1978;272:226.
[33] Juska T, Harrison IR. Polym Eng Sci 1982;22:766.
[34] Popli R, Mandelkern L. J Polym Sci Polym Phys Ed 1987;25:441.
[35] Wu W, Wignal GD, Mandelkern L. Polymer 1992;33:4137.
[36] Peterlin A, Meinel G. Makromol Chem 1971;142:227.
[37] Meinel G, Peterlin A. Colloid Polym Sci 1970;242:1151.
[38] Corneliussen R, Peterlin A. Makromol Chem 1967;105:193.
[39] Hiss R, Hobeika S, Lynn C, Strobl G. Macromolecules 1999;32:4390.
[40] Butler MF, Donald AM, Ryan A. Polymer 1997;38:5521.
[41] Liu LZ, Hsiao BS, Fu BX, Ran SF, Toki S, Chu B, et al. Macromolecules 2003;36:1920.
[42] Kasal N, Kakudo M. J Polym Sci Part A 1964;2:1955.
[43] Hay IL, Keller A. J Mater Sci 1967;2:538.
[44] Cowking A, Rider JG, Hay IL, Keller A. J Mater Sci 1968;3:646.
[45] McConkey BH, Darlington MW, Saunders DW, Cannon CG. J Mater Sci 1971;6:572.
[46] Crist B, Fisher CJ, Howard PR. Macromolecules 1989;22:1709.
[47] Kiho H, Peterlin A, Geil PH. J Polym Sci 1965;B3:157.
[48] Sadler DM, Barham PJ. Polymer 1990;31:36.
[49] Sadler DM, Barham PJ. Polymer 1990;31:43.
[50] Sadler DM, Barham PJ. Polymer 1990;31:46.
[51] Swan PR. J Polym Sci 1962;56:403.
[52] Fleissner M. Kunststoffe 1987;77:45.
[53] Pawlak A. Polymer 2007;48:1347.
[54] Wunderlich B. Macromolecular physics, vol. 1. New York: Academic Press; 1973.
[55] Hobeika S, Men Y, Strobl G. Macromolecules 2000;33:1827.
[56] Al-Hussein M, Strobl G. Macromolecules 2002;35:8515.
[57] Peterlin A, Baltá-Calleja FJ. Kolloid Z Z Polym 1970;242:1093.
[58] Stribeck N. X-ray scattering of soft matter. Heidelberg: Springer; 2007.
[59] Glatter O, Kratky O. Small-angle X-ray scattering. London: Academic Press; 1982.
[60] Strobl G. Prog Polym Sci 2006;31:398.
[61] Takahashi Y, Ishida T. J Polym Sci Polym Phys 1988;26:2267.
[62] Yamada M, Miyasaka K, Ishikawa K. J Polym Sci 1971;A29:1083.
[63] Hong K, Strobl G. Macromolecules 2006;39:268.
[64] Polanyi M. Z Phys 1921;7:149.
[65] Hermanns P, Platzek P. Kolloid Z 1939;88:68.
[66] Popli R, Glotin M, Mandelkern L. J Polym Sci Polym Phys Ed 1984;22:407.
[67] Alberola N, Cavaille JY, Perez J. Eur Polym J 1992;28:949.
[68] Men YF, Rieger J, Enderle HF, Lilge D. Macromolecules 2003;36:4689.
[69] Pick M, Lovell R, Windel A. Polymer 1980;21:1017.